

PAPER

HIS-TORIC: extending core ICRF wave simulation to include realistic SOL plasmas

To cite this article: S. Shiraiwa *et al* 2017 *Nucl. Fusion* **57** 086048

View the [article online](#) for updates and enhancements.

You may also like

- [Phase-space resolved measurement of 2nd harmonic ion cyclotron heating using FIDA tomography at the ASDEX Upgrade tokamak](#)
M. Weiland, R. Bilato, B. Geiger *et al.*
- [A positive-definite form of bounce-averaged quasilinear velocity diffusion for the parallel inhomogeneity in a tokamak](#)
Jungpyo Lee, David Smithe, John Wright *et al.*
- [Poloidal asymmetries due to ion cyclotron resonance heating](#)
Ye O Kazakov, I Pusztai, T Fülöp *et al.*

HIS-TORIC: extending core ICRF wave simulation to include realistic SOL plasmas

S. Shiraiwa, J.C. Wright, J.P. Lee and P.T. Bonoli

77 Massachusetts ave., Cambridge, MA 20139, United States of America

E-mail: shiraiwa@psfc.mit.edu

Received 21 February 2017, revised 11 May 2017

Accepted for publication 22 June 2017

Published 19 July 2017



Abstract

This paper presents a novel approach to incorporating an arbitrarily shaped edge scrape-off-layer (SOL) plasma and an ion cyclotron range of frequency (ICRF) antenna structure into existing core ICRF wave simulation models. We partition the entire computation domain into two sub-domains: a core and an edge region. Simulations in each domain are performed separately with appropriate numerical solvers. For the core, the TORIC ICRF solver (Brambilla 1999 *Plasma Phys. Control. Fusion* **41** 1) was modified to impose an essential (Dirichlet) boundary condition at its interface with the edge domain. In the edge, a finite element method is used to solve a cold collisional plasma model. The domains are then joined together using the continuity boundary condition for the tangential electric and magnetic fields at their interfaces (Hybrid Integration of SOL to TORIC: HIS-TORIC). The model developed here was tested using an ICRH H minority heating scenario on the Alcator C-Mod tokamak (Hutchinson *et al* 1994 *Phys. Plasmas* **1** 1511). The simulated pattern of core wave propagation agrees well with a standard TORIC simulation. This approach opens the possibility of using a realistic diverted SOL plasma and a complicated 3D RF antenna together with a rigorous hot core plasma model, while requiring only minimal modification to existing RF codes.

Keywords: RF, fullwave, toric, comsol

(Some figures may appear in colour only in the online journal)

1. Introduction

Waves in the ion cyclotron range of frequency (ICRF) are widely used for heating fusion plasmas [1]. A number of ICRF solvers have been developed to predict the propagation and absorption of ICRF waves in the hot core plasma region ('core solver') [2–4]. Significant efforts have been made to verify and validate these codes through code benchmarks [5, 6] and experiments [7–9].

However, these core solvers use simplified models for scrape-off-layer (SOL) plasmas and an RF antenna. In particular, when a spectral expansion of radio frequency (RF) electric field is used to represent the spatially dispersive nature of hot plasma conductivity, it is difficult to handle the complex geometry typical of the SOL plasmas and RF antennas, and various levels of geometric simplification are necessary. In the case of the TORIC ICRF solver [2], a tokamak geometry is meshed using the flux coordinate system and the RF

electric field is expanded in Fourier modes in the poloidal and toroidal directions. This meshing scheme is inconsistent with the geometry of SOL plasmas on open field lines and antenna structures, and in fact the antenna is modeled as a current sheet aligned on a flux surface.

Antenna-plasma coupling codes ('edge solvers') have been developed independently from the core solvers. Various coupling codes with different levels of fidelity to RF physics and SOL/antenna geometry have been developed for waves in lower hybrid (LH) and ion cyclotron frequency ranges [10–14]. Some codes employ the finite element method (FEM) or the boundary element method (BEM) to account for the complicated three dimensional antenna geometry, which is reproduced as closely as possible to engineering CAD designs. However, these coupling simulations often only dealt with the region directly in front of antenna and/or use a radiating boundary condition, thereby ignoring the RF power reflected back from the core region. An important exception

worth mentioning in this regard is the TOPICA code [10] in which the response of the hot core region is introduced as a surface response computed by the FELICE code [15], and a possibility of using TORIC code to improve the plasma load model was also explored [16].

Reducing core impurity contamination has been a long-standing issue for the ICRF heating [17–19]. These recent experiments highlight that our ability to predict the antenna-plasma coupling accurately is limited by our understanding of the linear and non-linear interaction between the SOL plasma and the applied RF power. Obtaining the self-consistent picture of RF wave field that includes both core and edge regions would be the first step toward such a goal.

In the present work, we construct a solution of the RF field that includes both core and edge regions, by connecting the two regions via continuity conditions after first solving each region separately. This ‘domain partitioning’ approach contrasts with other approaches developed in previous works. In [20], Vsim (particle-in-cell, finite difference time domain solver) was used to model an ICRF wave in a half of the Alcator C-Mod tokamak plasma. In [21], the AORSA 2D simulation domain was expanded to the vacuum wall including the SOL plasmas. In the LHEAF fullwave code for LH wave propagation and absorption, an FEM representation was used in the entire poloidal cross-section of the tokamak plasma and a kinetic power absorption was introduced as a perturbation to the conductivity [22, 23]. While all of these works were at least partially successful in expanding the existing RF simulation capability to include both core and edge regions, none of them represents an ICRF/LH simulation which simultaneously includes a hot core plasma, surrounding cold SOL plasmas and a complicated 3D antenna structure all together.

Our approach first solves each core and edge region separately with a set of assumed boundary conditions, thereby generating an ensemble of solutions (‘mode solutions’) for each region (see an example of mode solutions in figure 2). We then construct an integrated solution of the combined SOL/core system from an appropriate superposition of the mode solutions, making use of the superposition principle of Maxwell’s equations (equation (1)). The weights given to each of mode solutions in the superposition are determined by a boundary condition: at the interface between core and edge regions, the tangential components of the RF electric and magnetic fields must be continuous. We use TORIC for the core region. TORIC requires only minimal modification to accommodate the boundary condition to build the mode solutions. We employ the FEM discretization for the edge region and used COMSOL Multiphysics [24] to solve the wave propagation in cold collisional plasmas and to assemble the mode solutions. Although we focus on solving a problem defined on a 2D poloidal cross-section with a single toroidal mode for the sake of simplicity, our boundary connection equation (discussed in section 2.3) is generic, and is applicable to the three dimensional case and waves in other frequency ranges.

The plan of this paper is as follows. The formulation of the approach is presented in section 2. Numerical implementation using TORIC and COMSOL Multiphysics is described in section 3. Section 4 presents the simulation results and a

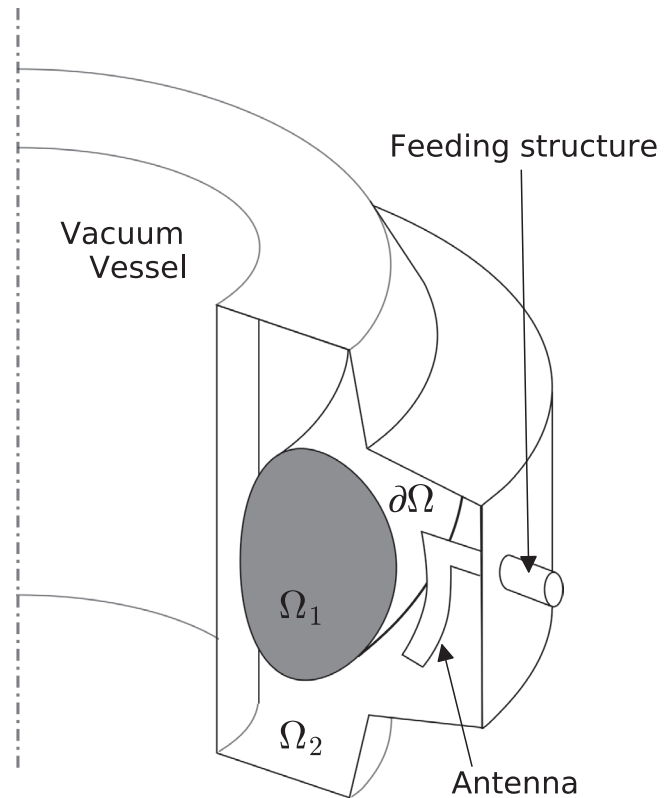


Figure 1. Schematics of the 3D ICRF problem and the ‘geometry partitioning’ approach. The core region (Ω_1) and the edge region (Ω_2) are separated by a smooth surface $\partial\Omega$. The antenna and RF power feeding structures are located in the domain Ω_2 and the RF power is fed to Ω_1 only through the surface $\partial\Omega$.

comparison to the simulation performed by the regular TORIC solver without including the FEM region. After discussing advantages and disadvantages of this approach in section 5, we conclude this paper in section 6.

2. Domain partitioning approach

2.1. Boundary condition (BC) for between core and edge regions

We consider an RF wave propagation problem in the toroidal geometry shown in figure 1 and solve the boundary problem of Maxwell’s equation in the frequency domain.

$$\nabla \times \mu^{-1}(\nabla \times \mathbf{E}) - \omega^2 \epsilon \mathbf{E} = j\omega \mathbf{J}_A, \quad (1)$$

where ω , ϵ , μ and \mathbf{J}_A are the wave angular frequency, the complex plasma dielectric permittivity, the magnetic permeability, and the antenna external current, respectively. The computation domain is surrounded by a vacuum vessel including an RF feedthrough that delivers RF power. The boundary conditions (BCs) must be specified on the vacuum wall and at the RF feed-through; the latter is represented by either a coaxial or waveguide port, which constrains forward RF power, or by a surface current boundary condition. We divide the entire computation domain into two separate sub-domains Ω_1 (core) and Ω_2 (edge) by a smooth closed surface $\partial\Omega$. The core domain Ω_1 is completely contained within the surface $\partial\Omega$, and RF power to it is fed only through the surface $\partial\Omega$.

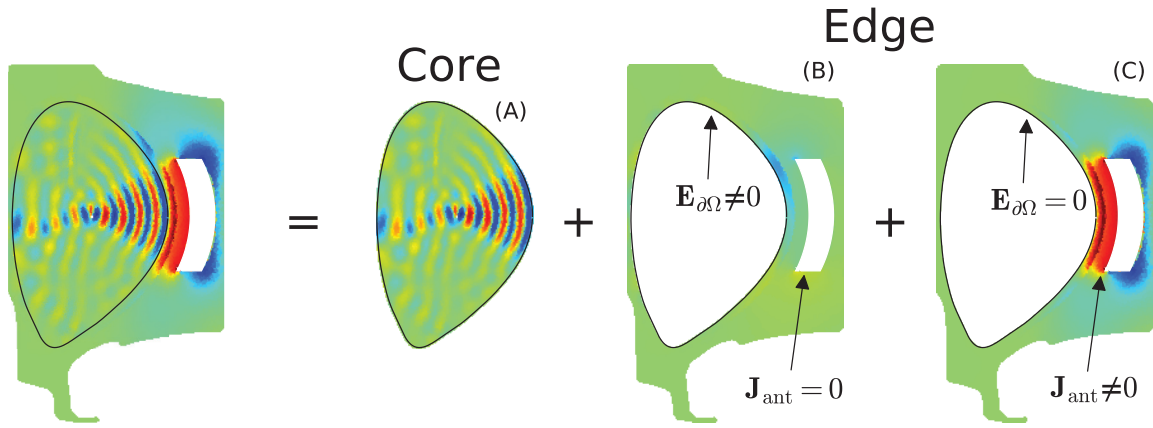


Figure 2. Domain partitioning approach. The original problem (left) is geometrically partitioned into core and edge sub-domains. The sub-domain solution for the edge is further decomposed into two solutions (B) and (C) and reconstructed on the basis of superposition principle.

Our approach is based on the recognition that equation (1) can be solved independently in both Ω_1 and Ω_2 , if we impose an essential boundary condition [25] on the separating surface $\partial\Omega$. Thus, the original problem of solving equation (1) for the entire domain reduces to developing the appropriate boundary condition on $\partial\Omega$ which allows one to join the sub-domain solutions to recover the whole solution. Figure 2 illustrates this domain partitioning approach in the 2D model. Note that in the 2D simulation example shown in figure 2, the external RF power source is represented as a surface current on a current strap (J_{ant}).

Generally, when two dielectric media share a common boundary ($\partial\Omega$ in our case) and when there is no surface current on the boundary, Maxwell's equations require the tangential components of fields to be continuous on the boundary. Since we chose $\partial\Omega$ to be smooth, we can represent the tangential field components on $\partial\Omega$ as Fourier series,

$$\mathbf{E}_t(\theta, \phi) = \sum_{(m,n)} (e_\eta^{m,n} \mathbf{u}_\eta + e_\zeta^{m,n} \mathbf{u}_\zeta) e^{im\theta + in\phi}, \quad (2)$$

$$\mathbf{B}_t(\theta, \phi) = \sum_{(m,n)} (b_\eta^{m,n} \mathbf{u}_\eta + b_\zeta^{m,n} \mathbf{u}_\zeta) e^{im\theta + in\phi}, \quad (3)$$

where θ and ϕ are poloidal and toroidal angles, η and ζ are coordinates on $\partial\Omega$ and \mathbf{u}_η and \mathbf{u}_ζ are the corresponding unit length tangential vectors. These unit vectors are functions of θ and ϕ . The poloidal mode number (m) extends from $-m_{max}$ to $+m_{max}$, and the toroidal mode number (n) extends from $-n_{max}$ to $+n_{max}$. Then, the continuity of the tangential electric and magnetic field components can be expressed as relationships among the Fourier coefficients

$$\begin{aligned} e_\eta^{m,n(1)} &= e_\eta^{m,n(2)}, \\ e_\zeta^{m,n(1)} &= e_\zeta^{m,n(2)}, \end{aligned} \quad (4)$$

$$\begin{aligned} b_\eta^{m,n(1)} &= b_\eta^{m,n(2)}, \\ b_\zeta^{m,n(1)} &= b_\zeta^{m,n(2)}, \end{aligned} \quad (5)$$

where the number in the parenthesis of the superscript denotes the sub-domain.

2.2. Fourier decomposition of solution

The boundary conditions given by equations (4) and (5) are not (yet) useful, because they simply relate the Fourier representation of BCs for Ω_1 to the corresponding Fourier representation of Ω_2 . Thus, it would appear that the problem of solving equation (1) for one sub-domain is not independent from the solution in the other sub-domain. To resolve this issue, we employ the concept of 'mode solutions' below and we will express a solution for an arbitrary electric field on $\partial\Omega$ as a weighted sum of 'mode solutions'.

We first solve equation (1) numerically in Ω_1 for a single Fourier mode on $\partial\Omega$. By solving the same problem for all possible Fourier modes on $\partial\Omega$, we construct a set of solutions ('mode solution'), as shown in figure 3. For a given (m, n) , there are two mode solutions, since there are two directions of the tangential electric field (\mathbf{u}_η and \mathbf{u}_ζ). We denote them as $\mathbf{E}_\eta^{m,n}(\mathbf{x})$ and $\mathbf{E}_\zeta^{m,n}(\mathbf{x})$, where \mathbf{x} is a position vector in Ω_1 and the subscript indicate the direction of applied boundary electric field. Note that these are vector fields. For example, the former has only a \mathbf{u}_η component on the surface $\partial\Omega$, but it can have all three components (\mathbf{u}_ψ , \mathbf{u}_η and \mathbf{u}_ζ) inside the domain Ω_1 . Then, when an arbitrary tangent electric field is given on the boundary $\partial\Omega$, we can compute the solution in Ω_1 as the weighted sum of the individual mode solutions,

$$\mathbf{E}^{m,n}(\mathbf{x}) = \sum_{(m,n)} \left[w_\eta^{m,n} \mathbf{E}_\eta^{m,n}(\mathbf{x}) + w_\zeta^{m,n} \mathbf{E}_\zeta^{m,n}(\mathbf{x}) \right], \quad (6)$$

where the weights ($w_\eta^{m,n}$ and $w_\zeta^{m,n}$) are equal to the Fourier coefficients of the boundary electric field, which corresponds to $e_\eta^{m,n}$ and $e_\zeta^{m,n}$ in equation (2). This corresponds to (A) in figure 2.

In the edge region Ω_2 , we need to take into account the external source, and therefore the solution is obtained from the sum of two parts. One part is a Fourier sum similar to that computed in Ω_1 . However, in Ω_2 , we need to impose not only a single Fourier mode on $\partial\Omega$ but also the zero external source on the RF feed-through. This corresponds to (B) in figure 2. The other part is a solution of the problem for which there is zero electric field on $\partial\Omega$ and a finite external source amplitude is imposed ('excitation mode'). This solution corresponds to (C) in figure 2.

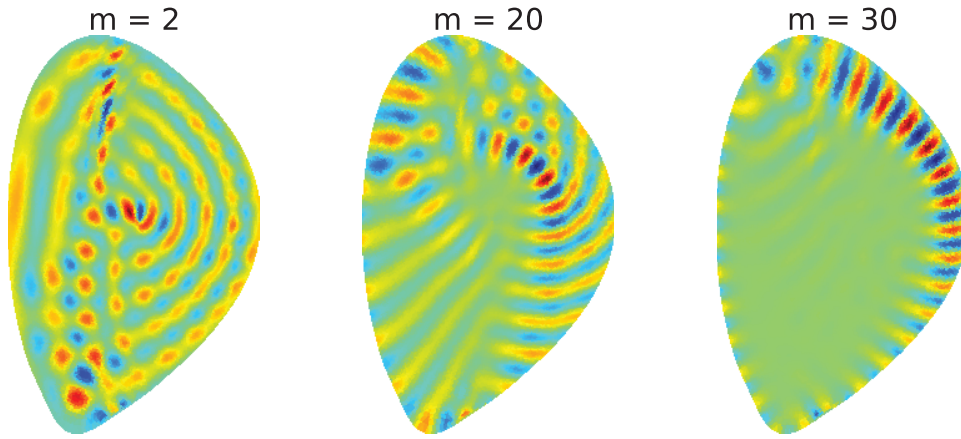


Figure 3. Example of mode solutions for $m = 2, 20$, and 30 , and $n = 10$. $\mathbf{u}_\eta e^{im\eta + in\zeta}$ is applied on $\partial\Omega$ and the η component of numerically obtained $\mathbf{E}_\eta^{m,n=10}(\mathbf{x})$ is shown. The simulation model and definition of η is given in section 3.

2.3. Boundary connecting equation

In the previous section, we decomposed the solution of the original problem as the sum of three families of solutions ((A)–(C) in figure 2), each of which can be obtained independently by solving a problem defined in either Ω_1 or Ω_2 . The remaining problem is to derive an equation that determines these weights from the BCs given by equations (4) and (5).

In order to use equations (4) and (5), we first define the response matrices,

$$\mathbf{G} \equiv \begin{bmatrix} \mathbf{G}_{\eta\eta} & \mathbf{G}_{\eta\zeta} \\ \mathbf{G}_{\zeta\eta} & \mathbf{G}_{\zeta\zeta} \end{bmatrix} \quad (7)$$

and the antenna excitation vector,

$$\mathbf{B}_{\text{ant}} \equiv [\mathbf{B}_{\text{ant } \eta}, \mathbf{B}_{\text{ant } \zeta}]^t, \quad (8)$$

where a row of sub-matrix \mathbf{G}_{ij} are the Fourier coefficients of the i direction of boundary magnetic field, when the electric field is imposed in the j direction. The boundary magnetic field is evaluated from $i\nabla \times \mathbf{E}/\omega$ of the mode solutions on the basis of Faraday's law. $\mathbf{B}_{\text{ant } i}$ are the Fourier coefficients of the i direction of boundary magnetic field of 'excitation mode'. Note that the elements of the response matrix and excitation vector are evaluated from solutions which can be obtained independently. We also introduce a notation for weights as $\mathbf{w} = [\mathbf{w}_\eta, \mathbf{w}_\zeta]^t$, where $\mathbf{w}_\eta = [w_\eta^{m,n}]$, $\mathbf{w}_\zeta = [w_\zeta^{m,n}]$.

Because the response matrices are associated with tangential fields, using these notations, the continuity of tangential magnetic field (equation (5)) can be written as follows.

$$\mathbf{G}^{(1)} \mathbf{w}^{(1)} = \mathbf{G}^{(2)} \mathbf{w}^{(2)} + \mathbf{B}_{\text{ant}}^{(2)}, \quad (9)$$

where $\mathbf{w}^{(1)}$ and $\mathbf{w}^{(2)}$ are the weights of superposition for Ω_1 and Ω_2 , respectively. From the continuity of electric field (equation (4)), it is obvious that $\mathbf{w}^{(1)} = \mathbf{w}^{(2)}$, since the electric field on $\partial\Omega$ is zero in 'excitation mode'. Therefore, we can determine \mathbf{w} from the following equation,

$$\mathbf{w} = (\mathbf{G}^{(1)} - \mathbf{G}^{(2)})^{-1} \mathbf{B}_{\text{ant}}^{(2)} \quad (10)$$

3. HIS-TORIC: integration of 2D SOL model to TORIC

We implemented the method described in the previous section, to add the edge regions (SOL plasmas and antenna) represented by an unstructured mesh to the TORIC ICRF solver (Hybrid Integration of SOL to TORIC: HIS-TORIC, where hybrid indicates the mixed use of spectral and FEM discretization). In the present implementation, both core and edge domains are assumed to be toroidally symmetric, which allows for solving the problem for a single toroidal mode number. The combined geometry is illustrated in figure 4, in which the TORIC core region is surrounded by arbitrarily shaped 2D SOL plasma and vacuum vessel. The connecting boundary between core and edge regions is chosen at the flux surface of the normalized poloidal flux (ψ) of 0.99. Note that we chose this location, because the physics assumptions used in both core as well as edge regions are valid. In particular it is important to select the connecting boundary 'cold' enough. Since hot plasma admits three modes, while there is only two modes in a cold plasma, it could be a source of error if the connecting boundary is hot enough. In the simulations shown in this work, the boundary temperature is set to 500 eV, for which $k_\perp \rho_i$ remains small.

We modified the TORIC solver to permit the imposition of the modal electric field excitation at a boundary coincidental with the matching flux surface, while the region external to that, including the vacuum, antenna and wall, are dropped. Each modal excitation corresponds to a single right hand side for the stiffness matrix [26], and the solver is able to solve for all needed excitation in a single run resulting in a computational cost of approximately only 2–3 times larger than a normal simulation. Mathematically, the required modification in TORIC is very similar to what was needed when it was attempted to use TORIC in order to build more realistic surface impedance boundary for the TOPICA code [16]. Indeed, we reused some subroutines from the work.

For the edge region, we used a cold plasma approximation [27] and took the collisional absorption due to electron-ion collisions into account by adding small imaginary part to particle mass [28, 29]. In the model geometry shown in figure 4,

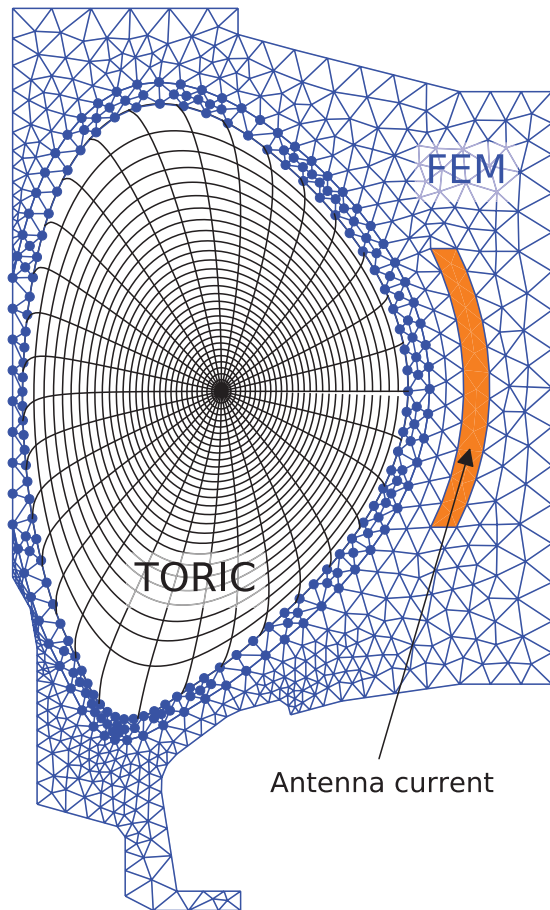


Figure 4. Schematics of geometry and mesh of 2D ICRF problem. In the edge region, blue marker indicated the region where cold SOL plasma exists.

the SOL plasma has a thickness of 2.5 cm. We set the density at the connecting boundary as the same as outer most flux surface density in the TORIC region and made a plasma density profile which exponentially decreases as a function of distance from the connecting boundary. For the magnetic field, we used an equilibrium magnetic field computed by EFIT [30] for computing the cold plasma dielectric tensor. In the previous section, the coordinate system used to express the RF field on the connecting boundary was arbitrary. TORIC uses the equal poloidal arc length flux coordinate system and a physical basis unit vectors ($\mathbf{u}_\psi \sim \nabla\psi$, $\mathbf{u}_\eta \sim \mathbf{B} \times \nabla\psi$, and $\mathbf{u}_\zeta \sim \mathbf{B}$), where ψ and \mathbf{B} are the normalized poloidal flux and static magnetic field, respectively. Since the dielectric property of magnetized plasma is anisotropic between the parallel and perpendicular directions with respect to the magnetic field, we chose η and ζ in TORIC for our coordinate system on the surface $\partial\Omega$. This choice eases the physics interpretation of simulation results. Because COMSOL uses the cylindrical coordinate system (r, ϕ, z), we implemented the coordinate transformation from r and z to \mathbf{u}_η and \mathbf{u}_ζ in our COMSOL model.

Note that in figure 4, the mesh is coarsened for visualization purpose. In the actual simulations, the connecting boundary is meshed by equal arc-length 256 segments in TORIC corresponding to the maximum poloidal mode number of 63. Radial mesh size in the core region is 240. On the FEM side,

the connecting boundary was meshed twice dense (512 segments) and the entire area was meshed by unstructured triangles. We use a rather low mesh growth rate so that size of triangles are nearly constant near the core and increases very slowly as approaching toward the vacuum vessel wall.

4. Verification using regular TORIC simulation

We have tested our implementation using an H minority heating scenario on Alcator C-Mod. An equilibrium from Alcator C-Mod (the toroidal field of $B_t = 5.4$ T and the plasma current of $I_p = 600$ kA) is used. Analytic temperature/density profiles with the central density of $n_{e0} = 5 \times 10^{20} \text{ m}^{-3}$ and the central temperature of $T_{e0} = 2$ keV, and a 5% concentration of H-minority with $T_{H0} = 120$ keV, based on [31], are used. In total, 254 modes (from $m = -63$ to $m = 63$ for both η and ζ directions) were used in this test. The toroidal mode number of $n = 10$ is used.

One may view the response matrix (equation (7)) as an admittance matrix of an RF network [32], which is closely relating to the scattering matrix and determines the coupling strength between different modes. Figure 5 shows the magnitude of core and edge response matrices, $|\mathbf{G}^{(1)}|$ and $|\mathbf{G}^{(2)}|$. It can be seen that the diagonal elements dominate in the edge region, while off-diagonal elements are more significant in the core region. This indicates that the coupling between different poloidal modes are stronger in the core region. On the contrary, in the edge region, most of the modes are not propagative modes and therefore the response appears strongly only in the diagonal elements.

Our mode solutions should form a complete set of functions to resolve the field solution. Figure 6 shows the amplitude of weights, $|\mathbf{w}|$, obtained from equation (9). The η component is much higher because the antenna strap current is in the poloidal direction and the pitch angle of magnetic field, $\arctan |B_\theta/B_\phi|$, is small. The amplitude is nearly symmetric with respect to $m = 0$ and decreases as the mode number increases. The amplitude of $|m| > 40$ modes is two orders of magnitude smaller than the $m = 0$ mode amplitude, indicating that sufficient resolution is obtained at 127 coupled modes for this particular case.

Figure 7 shows the amplitude of RF magnetic field modes at the surface $\partial\Omega$. Compared to the antenna excitation vector ($\mathbf{B}_{\text{ant}}^{(2)}$ in equation (9)), showing that the RF magnetic field mode spectrum becomes much broader due to the cross-mode coupling in the core region.

Figure 8 compares $E_- = (E_\psi - iE_\eta)/\sqrt{2}$ computed from the HIS-TORIC simulation to the one from a regular TORIC simulation, which uses a logically expanded (non physical) flux mesh outside the LCFS ignoring the actual magnetic geometry and retains a vacuum layer, simple antenna strap and conducting wall. In this particular scenario, in which the single pass power absorption is strong, the impact of how the SOL plasma and an antenna is considered to be small. Therefore, we do not expect a significantly different core wave propagation between the two simulations. Indeed, figure 8 shows that the wave field pattern computed by both methods are quite similar

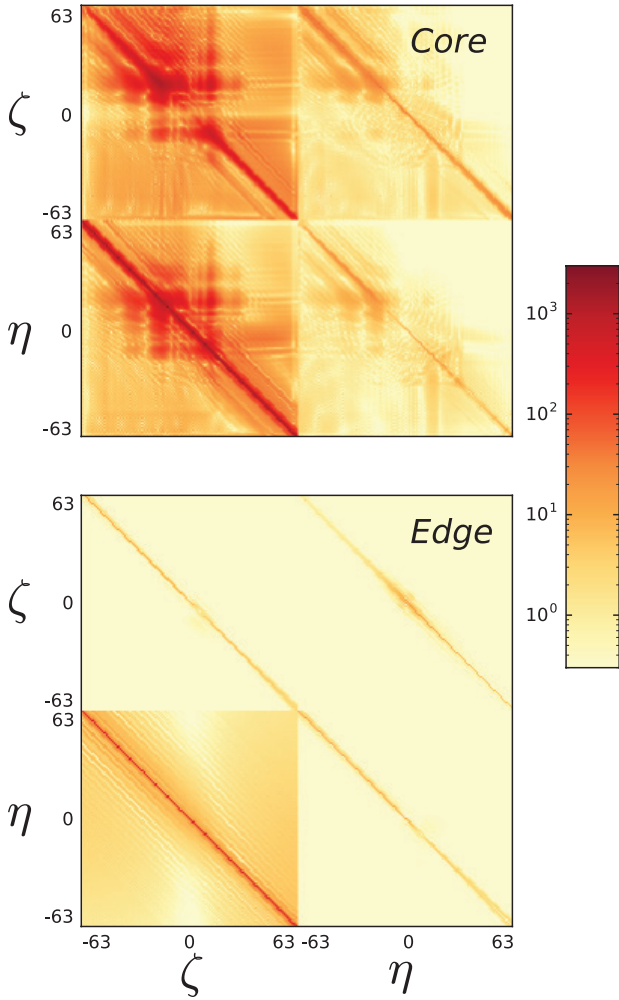


Figure 5. Magnitudes of core and edge response matrix ($|\mathbf{G}^{(1)}|$ and $|\mathbf{G}^{(2)}|$).

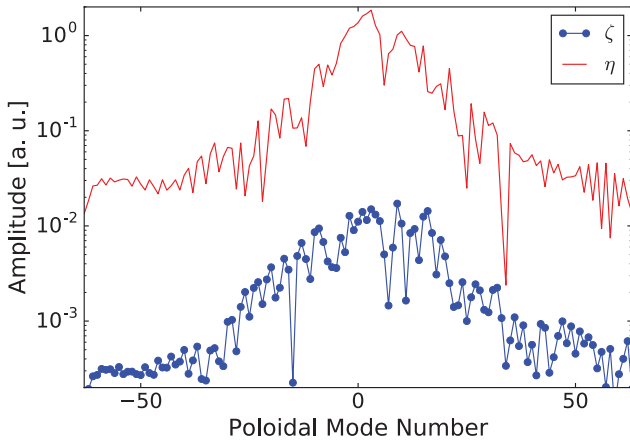


Figure 6. Amplitude of weights w for the η component (red) and the ζ component (blue).

in the core region. However, the edge region looks different. While the HIS-TORIC solution shows evanescent field excited only in front of the antenna strap, the regular TORIC shows side lobes due to the Fourier representation of antenna current.

The boundary connecting equation (equation (9)) derived from the continuity condition imposes no explicit condition on

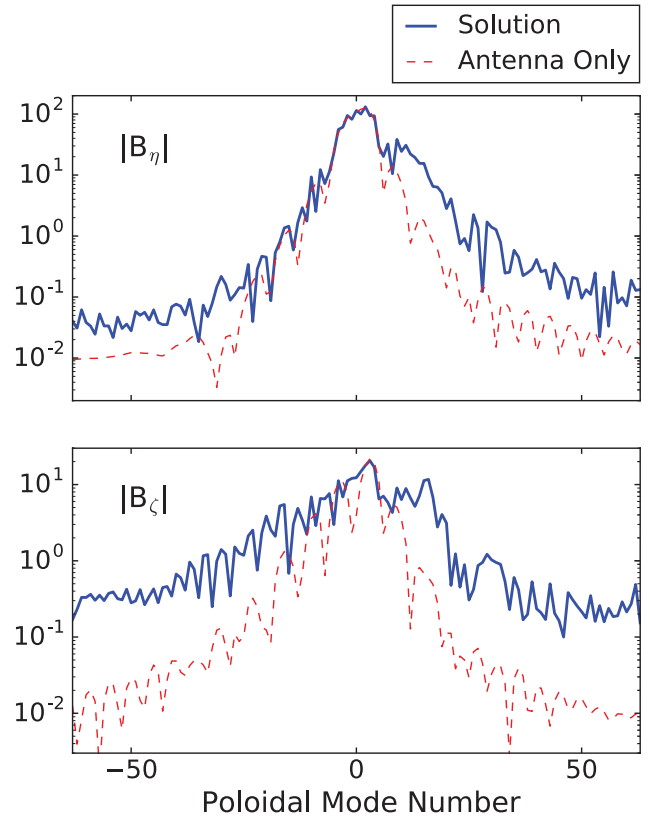


Figure 7. Comparison of RF magnetic field mode amplitudes evaluated from solution (blue) and antenna current alone (red).

how the perpendicular component behaves on the boundary. Since the density and magnetic field, and therefore a cold plasma dielectric, are chosen to be continuous, the continuity of radial component provides a way for inspecting precision of the solution. Figure 9 shows the computed E_ψ profiles and demonstrates that the radial field is also continuous at the core/edge connecting boundary. On the contrary, at the plasma-vacuum boundary (red dashed curve), the figure shows that the radial component becomes discontinuous because of the discontinuity of dielectric property.

5. Discussion

In the previous section, we used a thin-shell SOL plasma to keep the geometry similar to what is used in a regular TORIC simulation, which is shown in figure 8 (right). However, nothing prevents us from using a more realistic diverted SOL plasma. For the sake of demonstrating such capability, an H-minority heating scenario on a diverted C-Mod plasma was performed (figure 10). In this demonstration, we set up the density profile shown in the inset of figure 10 by solving a simple diffusion model assuming that the parallel diffusion is 1000 times larger compared to the perpendicular diffusion. The scale length of computed density profile on the low field side mid-plane is in the order of 1cm, which is consistent with observations (for example figure 3 in [33]). In a future work, the density and temperature profiles computed by more advanced model or the ones obtained from an experiment will be used.

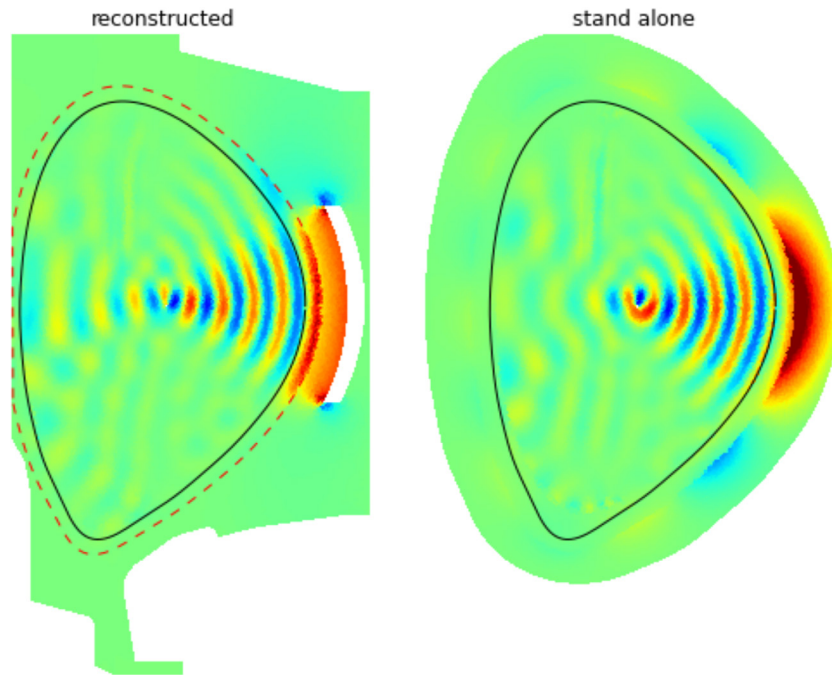


Figure 8. Comparison of E_{\perp} field computed by HIS-TORIC (left) and a regular TORIC code (right).

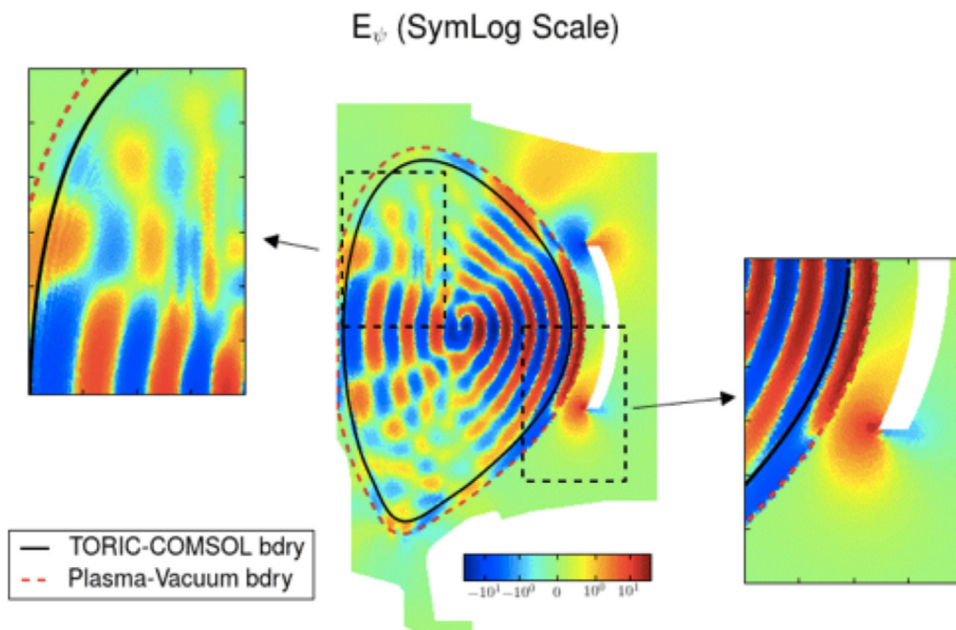


Figure 9. Profile of radial component of RF electric field (E_{ψ}). Black curves is the core/edge connecting boundary, where two solutions are connected. Red curves are the vacuum/plasma boundary. Two expanded views, one from near the antenna and one from the region away from the antenna both show that E_{ψ} is continuous on the connecting boundary.

It is important to note that while the electric field can be obtained from a superposition of the mode solutions, the power absorption should be evaluated using the reconstructed field in the full kinetic model of the core solver. We implemented an extension in a TORIC, so that it can use an arbitrary edge electric field spectrum at the surface $\partial\Omega$, in order to evaluate the core power absorption (see figure 11). The total power coupled to the core is determined by TORIC reconstruction is 16W as compared to 15.3W from the Poynting flux evaluated on the connecting boundary. Note that 1 A of current is used

in the antenna in this simulation so the 16W number when normalized to the antenna current give 16 Ohms of antenna coupling resistance, which is consistent with experimental measurements for an L-mode [34].

Although it involves solving the boundary value problem many times for different essential boundary conditions, the stiffness matrices remain the same. Both the TORIC core solver and the multifrontal massively parallel sparse direct solver (MUMPS) [35] used in the edge simulations support solving a linear system for multiple right hand sides. Therefore,

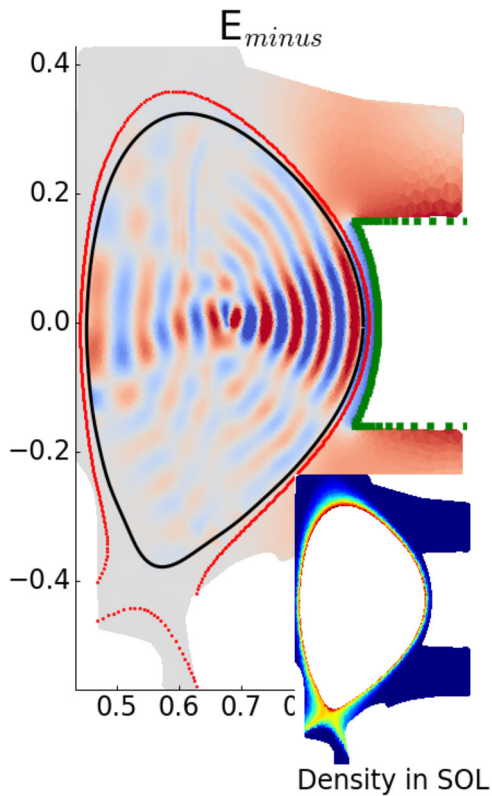


Figure 10. Core/Edge integrated simulation of Alcator C-Mod diverted tokamak plasma. E_- and the density profile (inset) is shown.

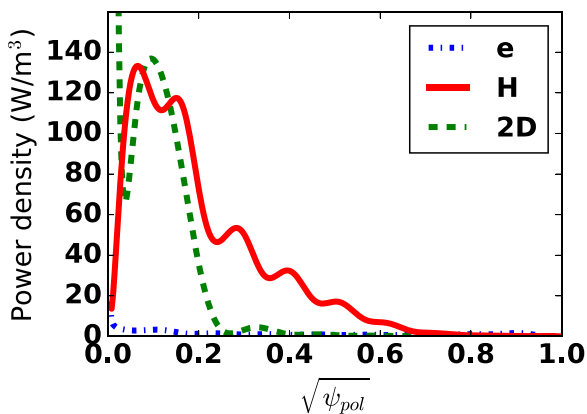


Figure 11. Profiles of RF power density deposited in different species versus the square root of normalized poloidal flux for the simulation shown in figure 8 (left). The total power absorbed in the core is 16.0 Watts. 66.6% of the power is in the fundamental H , 25.4% in the 2nd harmonic D , and remaining 9.0% in electrons.

additional computational costs of solving equation (9) and filling the response matrices remains modest. For example, for the simulation shown in figure 8, while running the regular TORIC simulation took 1.4 cpu hrs on our cluster, computing the 257 core mode solutions took 4.4 cpu-hrs.

While we focused on verifying our formalization of connecting two regions to obtain physically consistent RF field, the eventual goal of this extension is to investigate the situation where RF propagation in the edge region may impact core RF heating/current drive and antenna coupling significantly.

Here, we would discuss our perspective of issues which our core/edge domain partitioning approach can address in future. Wave single pass power absorption in ICRF mode-conversion scenario is relatively small, and therefore it is expected that a relatively larger RF wave field is excited in SOL plasmas. A cold SOL plasma may contribute non-negligible power loss due to collisional absorption. It may also be possible that the 3D edge structure allows for coupling different toroidal modes and may result in significant modification of the effective antenna spectrum.

Our understanding of the linear and non-linear interaction between the SOL plasma is not yet sufficient to predict reliably the antenna-plasma coupling and the impurity generation and contamination [17–19]. For example, a study of core impurity contamination comparing a traditional toroidally aligned and a field aligned ICRF antenna reveals that measured RF-induced potentials are at the same level while core contamination was indeed lower when field aligned ICRF antenna is used [19]. This observation suggests a lack of understanding of the mechanism determining the SOL plasma potential in the presence of ICRF and its impact on impurity contamination and sources. Precise modeling of RF electric field excited in SOL region and complicated antenna structure is critical to advancing our understanding of this issue. With the RF field accurately modeled, we can proceed incorporating a simulation model to predict an RF rectified potential on material surface, such as the one studied in [36]. Not to mention, the antenna current on the field aligned antenna can not be decomposed by superposition of 2D poloidal currents with different toroidal modes. Therefore, accurate modeling of such antenna requires the inclusion of a 3D antenna geometry.

Lastly, we would like to emphasize the universality of this approach. Treating edge plasmas using a cold collisional model without including hot dielectric effects is likely to be valid for the LH waves and high harmonic fast waves (HHFWs) [37], also. Furthermore, the domain partitioning does not require the toroidal symmetry at all even in the core region. Therefore, the equation for the boundary connection would be extensible in other frequency ranges and even for a stellarator plasma.

6. Conclusion

In this paper, we extended the TORIC core spectral ICRF solver to incorporate the edge region consisting from arbitrarily shaped SOL plasmas, the antenna current strap and the vacuum vessel. The edge region interfaces the core region on a flux surface, without an overlap, and is solved using FEM. We developed the following domain partitioning method: formulating both regions as a Maxwell boundary value problem with the essential BC on the connecting boundary; solving each region separately for all boundary Fourier modes; superimposing thus obtained ‘mode solutions’ to construct the solution. The reconstructed RF field needs to satisfy the continuity conditions given by equations (4) and (5), which in turn leads to the equation for the weights used in the superposition, equation (9). This method was tested using an Alcator C-Mod H-minority heating case. We confirmed that all RF field components are joined continuously at the boundary including the

radial component. The computed core RF field pattern was very similar to what was computed using a regular TORIC code, which is reasonable given a strong single pass absorption. A simulation using more realistic diverted SOL plasma geometry was also performed to demonstrate the capability of handling non-conformal SOL plasmas. The power deposition profiles are computed afterward using the reconstructed RF field. Our formulation is extensible to include 3D antenna structure, non-axisymmetric core plasmas such as a stellarator, and other frequency ranges such as LH and HHFW.

Acknowledgments

An author (S. Shiraiwa) thanks Dr. R. Bilato (IPP), Dr. O. Meneghini (GA), Dr. S. Wukitch (MIT), and Dr. Y. Lin (MIT) for the useful discussion about the TORIC solver and wave field boundary condition. Work supported by the US Department of Energy, Office of Science, Office of Fusion Energy Sciences, using User Facility Alcator C-Mod, under Award Number DE-FC02-99ER54512 and by US DoE Contract No. DE-FC02-01ER54648 under a Scientific Discovery Through Advanced Computing Initiative.

References

- [1] Perkins F.W. 1977 *Nucl. Fusion* **17** 1197
- [2] Brambilla M. 1999 *Plasma Phys. Control. Fusion* **41** 1
- [3] Jaeger E., Berry L., D'Azevedo E., Batchelor D., Carter M., White K. and Weitzner H. 2002 *Phys. Plasmas* **9** 1873–81
- [4] Fukuyama A., Yokota E. and Akutsu T. 2000 *Proc. 18th Int. Conf. on Fusion Energy (Sorrent)* (IAEA: Vienna) CD-ROM (<http://iaea.org/programmes/ripc/physics/fec2000/html/node1.htm>)
- [5] Bilato R. et al 2014 *AIP Conf. Proc.* **1580** 291
- [6] Bilato R., Bertelli N., Brambilla M., Dumont R., Jaeger E., Johnson T., Lerche E., Sauter O., Van Eester D. and Villard L. 2015 *AIP Conf. Proc.* **1689** 060001
- [7] Lin Y. et al 2005 *Plasma Phys. Control. Fusion* **47** 1207
- [8] Bader A., Granetz R., Parker R., Bonoli P., Hutchinson I., Sears J. and Wukitch S. 2012 *Nucl. Fusion* **52** 094019
- [9] Tsujii N., Porkolab M., Bonoli P., Lin Y., Wright J., Wukitch S., Jaeger E., Green D. and Harvey R. 2012 *Phys. Plasmas* **19** 082508
- [10] Lancellotti V., Milanesio D., Maggiora R., Vecchi G. and Kyrtsya V. 2006 *Nucl. Fusion* **46** S476
- [11] Hillairet J., Voyer D., Ekedahl A., Goniche M., Kazda M., Meneghini O., Milanesio D. and Preynas M. 2010 *Nucl. Fusion* **50** 125010
- [12] Milanesio D., Meneghini O., Maggiora R., Guadamuz S., Hillairet J., Lancellotti V. and Vecchi G. 2011 *Nucl. Fusion* **52** 013008
- [13] Meneghini O., Lau C., Shiraiwa S., Wallace G.M., Parker R.R., LaBombard B.L., Faust I.C., Wilson J.R., and Wukitch S.J. 2011 *AIP Conf. Proc.* **1406** 411–8
- [14] Preynas M., Goniche M., Hillairet J., Litaudon X., Ekedahl A. and Colas L. 2013 *Nucl. Fusion* **53** 013012
- [15] Brambilla M. 1989 *Plasma Phys. Control. Fusion* **31** 723
- [16] Wright J.C., Bonoli P.T., Brambilla M., Bilato R., Maggiora R. and Lancellotti V. 2006 *33rd EPS Conf. on Plasma Physics (Rome, Italy, 19–23 June 2006)*
- [17] Jacquet P.A. et al 2011 *Nucl. Fusion* **51** 103018
- [18] Bobkov V. et al 2013 *Nucl. Fusion* **53** 093018
- [19] Wukitch S. et al 2013 *Phys. Plasmas* **20** 056117
- [20] Jenkins T.G. and Smithe D.N. 2015 *AIP Conf. Proc.* **1689** 030003
- [21] Green D.L., Berry L., Chen G., Ryan P., Canik J. and Jaeger E. 2011 *Phys. Rev. Lett.* **107** 145001
- [22] Meneghini O., Shiraiwa S. and Parker R. 2009 *Phys. Plasmas* **16** 090701
- [23] Shiraiwa S. et al 2011 *Phys. Plasmas* **18** 080705
- [24] Comsol B.A. Comsol multiphysics™, Stockholm, Sweden <http://comsol.com/>.
- [25] Jin J. 1993 *Finite Element Method in Electromagnetics* (New York: Wiley)
- [26] Bondeson A., Rylander T. and Ingelström P. 2000 *Computational Electromagnetics* (Berlin: Springer)
- [27] Stix T.H. 1992 *Waves in Plasmas* (New York: Springer)
- [28] Shiraiwa S., Meneghini O., Parker R., Bonoli P., Garrett M., Kaufman M.C., Wright J.C. and Wukitch S. 2010 *Phys. Plasmas* **17** 056119
- [29] Meneghini O. 2012 *PhD Thesis* Massachusetts Institute of Technology (<https://dspace.mit.edu/handle/1721.1/76501#files-area>)
- [30] Lao L., John H.S., Stambaugh R., Kellman A. and Pfeiffer W. 1985 *Nucl. Fusion* **25** 1611
- [31] Tang V. 2007 *Plasma Phys. Control. Fusion* **49** 873
- [32] Pozar D.M. 2005 *Microwave Engineering* 3rd edn (Hoboken, NJ: Wiley)
- [33] Lau C. 2013 *Plasma Phys. Control. Fusion* **55** 025008
- [34] Parisot A., Wukitch S.J., Bonoli P., Hughes J.W., LaBombard B., Lin Y., Parker R., Porkolab M. and Ram A.K. 2004 *Plasma Phys. Control. Fusion* **46** 1781
- [35] Amestoy P.R., Duff I.S. and L'Excellent J.Y. 2000 *Comput. Methods Appl. Mech. Eng.* **184** 501–20
- [36] Myra J.R. and D'Ippolito D.A. 2015 *Phys. Plasmas* **22** 062507
- [37] Ono M. 1995 *Phys. Plasmas* **2** 4075–82